Iron-Doped Carbon Aerogels: Novel Porous Substrates for Direct Growth of Carbon Nanotubes

Stephen A. Steiner, III,[†] Theodore F. Baumann,*[,‡] Jing Kong,[§] Joe H. Satcher, Jr.,[‡] and Mildred S. Dresselhaus[§,||]

Department of Materials Science and Engineering, Department of Electrical Engineering and Computer Science, and Department of Physics, Massachusetts Institute of Technology, Cambridge, Massachusetts 02139, and Chemistry, Materials, and Life Sciences Directorate, Lawrence Livermore National Laboratory, Livermore, California 94551

Received December 16, 2006. In Final Form: February 20, 2007

We present the synthesis and characterization of Fe-doped carbon aerogels (CAs) and demonstrate the ability to grow carbon nanotubes directly on monoliths of these materials to afford novel carbon aerogel−carbon nanotube composites. Preparation of the Fe-doped CAs begins with the sol−gel polymerization of the potassium salt of 2,4-dihydroxybenzoic acid with formaldehyde, affording K^+-doped gels that can then be converted to Fe^{2+}- or Fe^{3+}-doped gels through an ion exchange process, dried with supercritical CO_2, and subsequently carbonized under an inert atmosphere. Analysis of the Fe-doped CAs by TEM, XRD, and XPS revealed that the doped iron species are reduced during carbonization to form metallic iron and iron carbide nanoparticles. The sizes and chemical composition of the reduced Fe species were related to pyrolysis temperature as well as the type of iron salt used in the ion exchange process. Raman spectroscopy and XRD analysis further reveal that, despite the presence of the Fe species, the CA framework is not significantly graphitized during pyrolysis. The Fe-doped CAs were subsequently placed in a thermal CVD reactor and exposed to a mixture of CH_4 (1000 sccm), H_2 (500 sccm), and C_2H_4 (20 sccm) at temperatures ranging from 600 to 800 °C for 10 min, resulting in direct growth of carbon nanotubes on the aerogel monoliths. Carbon nanotubes grown by this method appear to be multiwalled (∼25 nm in diameter and up to 4 μm long) and grow through a tip-growth mechanism that pushes catalytic iron particles out of the aerogel framework. The highest yield of CNTs was grown on Fe-doped CAs pyrolyzed at 800 °C treated at CVD temperatures of 700 °C.

Introduction

Carbon aerogels (CAs) are novel mesoporous materials with many interesting properties, such as low mass densities, continuous porosities, high surface areas, and high electrical conductivity.[1−4] These properties are derived from the aerogel microstructure, which is a network of interconnected primary particles with characteristic diameters between 3 and 25 nm. CAs are typically prepared through the sol−gel polymerization of resorcinol with formaldehyde in aqueous solution to produce organic gels that are supercritically dried and subsequently pyrolyzed in an inert atmosphere. To expand the potential application for these unique materials, recent efforts have focused on the introduction of transition metals into CAs with the goal of modifying the structure, conductivity, or catalytic activity of the aerogel.[5−13] We previously reported the synthesis, characterization, and physical properties of a variety of metal-doped CAs.[14−18] These materials were prepared through the sol−gel polymerization of resorcinol derivatives containing metal-binding sites that allow for the uniform incorporation of metal ions into the organic gel structure. One of the interesting aspects of this approach is that certain transition metal ions, such as Co^{2+}, Ni^{2+}, and Cu^{2+}, are reduced during the carbonization process, leading to the formation of nanometer-sized metallic particles distributed throughout the carbon matrix. In addition, for the Co- and Ni-doped systems, these nanoparticles were found to catalytically induce a solid-state restructuring of the surrounding carbon framework into graphitic nanoribbons and other graphitic nanostructures. These observations led us to investigate the possibility of utilizing these supported metal nanoparticles as catalysts for the growth of carbon nanotubes (CNTs) within the porous CA structure. Such an approach could provide a new route to novel carbon-based composites with enhanced thermal, electrical, and mechanical properties. Unfortunately, for the Co- and Ni-doped CAs, the metal nanoparticles become encased in graphitic carbon during the carbonization process and, therefore,

* Corresponding author. E-mail: baumann2@llnl.gov.
† Department of Materials Science and Engineering, MIT.
‡ Lawrence Livermore National Laboratory.
§ Department of Electrical Engineering and Computer Science, MIT.
|| Department of Physics, MIT.

(1) Pekala, R. W. *J. Mater. Sci.* **1989**, *24*, 3221.
(2) Pekala, R. W.; Alviso, C. T.; Kong, F. M.; Hulsey, S. S. *J. Non-Cryst. Solids* **1992**, *145*, 90.
(3) Pekala, R. W.; Alviso, C. T.; LeMay, J. D. In *Chemical Processing of Advanced Materials*; Hench, L. L., West, J. K., Eds.; J. Wiley and Sons: New York, 1992; p 671.
(4) Kong, F. M.; LeMay, J. D.; Hulsey, S. S.; Alviso, C. T.; Pekala, R. W. *J. Mater. Sci.* **1993**, *8*, 3100.
(5) Bekyarova, E.; Kaneko, K. *Adv. Mater.* **2000**, *12*, 1625.
(6) Bekyarova, E.; Kaneko, K. *Langmuir* **1999**, *15*, 7119.
(7) Maldonado-Hódar, F. J.; Moreno-Castilla, C.; Rivera-Utrilla, J.; Hanzawa, Y.; Yamada, Y. *Langmuir* **2000**, *16*, 4367.
(8) Maldonado-Hódar, F. J.; Ferro-García, M. A.; Rivera-Utrilla, J.; Moreno-Castilla, C. *Carbon* **1999**, *37*, 1199.
(9) Moreno-Castilla, C.; Maldonado-Hódar, F. J.; Rivera-Utrilla, J.; Rodríguez-Castellón, E. *Appl. Catal., A* **1999**, *183*, 345.
(10) Moreno-Castilla, C.; Maldonado-Hódar, F. J. *Phys. Chem. Chem. Phys.* **2000**, *2*, 4818.
(11) Moreno-Castilla, C.; Maldonado-Hódar, F. J.; Carrasco-Marin, F.; Rodriguez-Castellon, E. *Langmuir* **2002**, *18*, 2295.
(12) Miller, J. M.; Dunn, B. *Langmuir* **1999**, *15*, 799.
(13) Fu, R.; Dresselhaus, M. S.; Dresselhaus, G.; Zheng, B.; Liu, J.; Satcher, J. H.; Baumann, T. F. *J. Non-Cryst. Solids* **2003**, *318*, 223.
(14) Baumann, T. F.; Fox, G. A.; Satcher, J. H.; Yoshizawa, N.; Fu, R.; Dresselhaus, M. S. *Langmuir* **2002**, *18*, 7073.
(15) Fu, R.; Yoshizawa, N.; Dresselhaus, M. S.; Dresselhaus, G.; Satcher, J. H.; Baumann, T. F. *Langmuir* **2002**, *18*, 10100.
(16) Fu, R.; Lin, Y. M.; Rabin, O.; Dresselhaus, G.; Dresselhaus, M. S.; Satcher, J. H.; Baumann, T. F. *J. Non-Cryst. Solids* **2003**, *317*, 247.
(17) Baumann, T. F.; Satcher, J. H. *Chem. Mater.* **2003**, *15*, 3745.
(18) Fu, R.; Baumann, T. F.; Cronin, S.; Dresselhaus, G.; Dresselhaus, M. S.; Satcher, J. H. *Langmuir* **2005**, *21*, 2647.

10.1021/la063643m CCC: $37.00
Published on Web 03/24/2007

are unable to function as catalysts for CNT growth. As a result, we sought alternative metal catalysts that could be prepared using our sol−gel method and that would remain active following carbonization. In this paper, we present the synthesis and characterization of Fe-doped CAs and demonstrate their effectiveness as catalysts for the formation of CNTs by chemical vapor deposition (CVD). Although the growth of CNTs on inorganic aerogel substrates has been previously reported,[19−30] our materials represent the first reported example of CNTs grown directly from CAs. We will describe the effect of CA preparation on the catalytic activity of Fe nanoparticles as well as the influence of CVD conditions on nanotube growth.

Experimental Procedures

Sample Preparation. The Fe-doped CAs were prepared by modification of our previously reported method.[14] In a typical experiment, a suspension of 2,4-dihydroxybenzoic acid (2.9 g, 18.8 mmol) in distilled water (100 mL) was treated with K_2CO_3 (1.29 g, 9.4 mmol) with vigorous stirring. The reaction solution became clear after 0.5 h, when all of the acid was neutralized. Formaldehyde (2.98 g, 37% w/v in water, 37 mmol) was then added along with an additional amount of K_2CO_3 (26 mg, 0.188 mmol) to serve as a polymerization catalyst. The solution was then stirred for 24 h, after which it was transferred to glass vials, sealed, and cured in an oven at 80 °C for 72 h. The resulting K^+-loaded gels were obtained as dark red, transparent monoliths. The gels were then removed from the molds, sliced into discs with a razor blade, and soaked in a solution of 0.1 M aqueous $Fe(NO_3)_3$, $FeCl_3$, $FeSO_4$, or $(NH4)_2$-$Fe(SO_4)_2$ for a total of 72 h, with fresh solution exchanged in every 24 h. The undoped gels were prepared by ion exchange of the K^+-doped gels with 0.1 M HCl. Ion exchanged gels were washed in deionized water for 72 h to remove any unbound iron species from the gels and then with acetone for 72 h to remove all water from the pores of the gel network. The wet gels were subsequently dried with supercritical CO_2 (31.1 °C and 7.38 MPa). The resulting undoped and Fe-doped organic aerogels were carbonized by pyrolysis at 600, 800, and 1050 °C under an N_2 atmosphere for 10.5 h. Pyrolyzed samples are denoted as DT_c, where D is the dopant (Fe or H) and T_c is the carbonization temperature. For CVD growth of CNTs, the Fe-doped CAs were placed in a 2.5 cm long segment of 1 cm diameter quartz tubing and inserted into the middle of a 2.7 cm inner diameter quartz process tube. The tube was flushed with Ar at a rate of 200 sccm for 20−40 min and then placed into a clamshell furnace preheated to a temperature ranging from 800 to 950 °C. The CVD treatment was then performed by exposure of the CA monoliths to a flow of 500 sccm H_2, 30 sccm CH_4, and 20 sccm C_2H_4, for 10 min performed at temperatures of either 600, 700, or 800 °C. The tube was then taken out of the furnace and allowed to cool under a flow of Ar (500 sccm). Each sample having undergone CVD is denoted as DT_c-T_d, where T_d is the CVD temperature.

Characterization. High-resolution transmission electron microscopy (HRTEM) of Fe-doped carbon aerogels and derived nanotube composites was performed on a JEOL JEM-200CX instrument operating at 200 keV. XRD spectra were obtained using a Rigaku 300 X-ray diffractometer operating with the following measurement parameters: high voltage = 60 kV; current = 300 mA; divergence slit = 1°; scatter slit = 2°; receiving slit = 0.6°; scan mode = continuous; scan type = standard; axis = $2\theta/\theta$; scan = 10−80°; scan speed = 0.25° min^{-1}; and sampling interval = 0.03°. Phase identification was made using MDI Jade 7 equipped with the ICSD and NIST databases of XRD spectra. XPS spectra were obtained on an AXIS HIS 165 and ULTRA spectrometer (Kratos Analytical Limited) using Al Kα radiation (energy = 1486.6 eV) in a vacuum of 5×10^{-9} Torr. Samples were prepared by grinding the CA material into a fine powder, adhering to adhesive copper tape, and mounting the copper tape on a sample holder using double-sided adhesive tape. X-ray slots of 750 × 350 μm, an X-ray power of 150 W (15 kV and 10 mA), and a pass energy of 80 eV for 100 sweeps were used for all measurements. Charge correction was performed for Fe600 samples, which were the only samples to exhibit any kind of charging effect. High-resolution scanning electron microscopy (HRSEM) was performed with a JEOL 6320 microscope operating at 5 kV. Raman spectra were obtained using a custom-built micro-Raman spectrometer operating at excitation wavelengths of 785, 676, 752, and 514 nm.

Results and Discussion

Iron-Doped Carbon Aerogels. Our objective in this work was to design a novel CA material that could support a catalyst for the CVD growth of CNT. In our previous work with the Co- and Ni-doped CAs, the metal nanoparticles in these materials became encased in graphitic carbon during the carbonization process,[18] and as a result, the catalytic sites were inaccessible to CVD gases. Iron was selected as the catalyst for this study because, like Co and Ni, iron-based compounds are known to efficiently catalyze the growth of carbon nanotubes.[31] In addition, since iron-carbon systems are rich in phases[32] (more so than cobalt or nickel), we hoped that this process would generate catalytic iron-containing nanoparticles, either iron metal or iron carbide, that would still be accessible and active after the carbonization process. The Fe-doped CAs investigated in this study were prepared by the same method used to synthesize the Co- and Ni-doped CAs. Specifically, the base-catalyzed sol−gel polymerization of a resorcinol derivative, the potassium salt of 2,4-dihydroxybenzoic acid, with formaldehyde afforded K^+-doped wet gels that could then be doped with iron through our ion exchange process with the following Fe^{2+} and Fe^{3+} salts: $FeSO_4$, $(NH_4)_2Fe(SO_4)_2$, $Fe(NO_3)_3$, or $FeCl_3$. After supercritical drying of the wet gels, the Fe-doped organic aerogels were then carbonized at temperatures ranging from 600 to 1050 °C.

To determine the types of Fe species that form during carbonization as well as their effect on the surrounding carbon network, the structure and composition of the Fe-doped CAs were evaluated using TEM, powder XRD, Raman spectroscopy, and XPS. TEM images of the Fe-doped CAs show that the aerogel structure consists of an interconnected network of primary carbon particles with diameters between 10 and 15 nm (Figure 1). In addition, metallic nanoparticles are evident throughout the carbon framework of the Fe-doped CAs, most easily seen in materials pyrolyzed above 800 °C. As with the Co- and Ni-doped CAs, the size distribution of the Fe nanoparticles is intimately tied to the carbonization temperature, with higher pyrolysis temperatures yielding a wider distribution of sizes. The composition of these metallic nanoparticles was examined using XRD. Interestingly,

(19) Li, X.; Yuan, G.; Brown, A.; Westwood, A.; Brydson, R.; Rand, B. *Carbon* **2006**, *44*, 1699.
(20) Li, X.; Zuo, X.; Yuan, G.; Brown, A.; Westwood, A.; Brydson, R.; Rand, B. *J. Phys.: Conf. Ser.* **2005**, *26*, 308.
(21) Zhang, D.; Shi, L.; Fang, J.; Li, X.; Dai, K. *Mater. Lett.* **2005**, *59*, 4044.
(22) Piao, L.; Chen, J.; Li, Y. *China Particuol.* **2003**, *1*, 266.
(23) Aslam, Z.; Li, X.; Brydson, R.; Rand, B. *Inst. Phys. Conf. Ser.* **2004**, *179*, 471.
(24) Ward, J. W.; Wei, B. Q.; Ajayan, P. M. *Chem. Phys. Lett.* **2003**, *376*, 717.
(25) Zheng, B.; Li, Y.; Liu, J. *Appl. Phys. A: Mater. Sci. Process.* **2002**, *74*, 345.
(26) Su, M.; Zheng, B.; Liu, J. *Chem. Phys. Lett.* **2000**, *322*, 321.
(27) Song, X.-Y.; Cao, W.; Ayers, M. R.; Hunt, A. J. *J. Mater. Res.* **1995**, *10*, 251.
(28) Song, X. Y.; Cao, W.; Hunt, A. J. *Mater. Res. Soc. Symp. Proc.* **1994**, *349*, 269.
(29) Cao, W.; Song, X. Y.; Hunt, A. J. *Mater. Res. Soc. Symp. Proc.* **1994**, *349*, 87.
(30) Hu, J.; Bando, Y.; Zhan, J.; Zhi, C.; Xu, F.; Golberg, D. *Adv. Mater.* **2006**, *18*, 197.
(31) For a recent review, see: Dupuis, A. *Prog. Mater. Sci.* **2005**, *50*, 929 and references therein.
(32) Shunk, F. A. *Constitution of Binary Alloys, Second Supplement*; McGraw-Hill: New York, 1969.

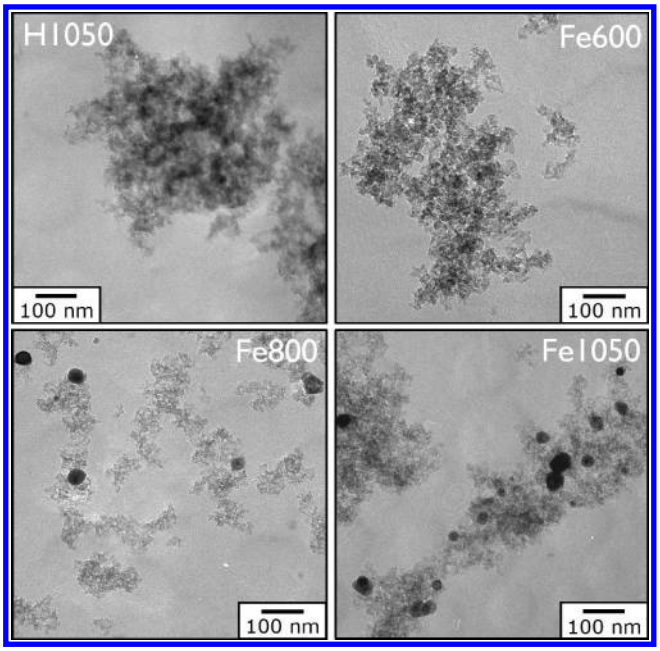

Figure 1. TEM micrographs of an undoped CA (H1050) and Fe-doped CAs pyrolyzed at different temperatures (Fe600, Fe800, and Fe1050).

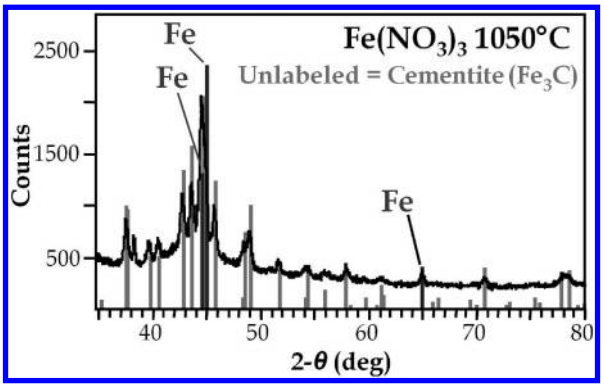

Figure 2. X-ray diffraction patterns for Fe-doped CAs prepared with $Fe(NO_3)_3$ and the expected peak positions and relative intensities for iron metal and the cementite phase of iron carbide (unlabeled gray peaks).

the type of Fe species that forms during pyrolysis appears to be related to the type of salt used for ion exchange. The XRD pattern for CAs doped with $Fe(NO_3)_3$ exhibited diffraction lines attributable to the presence of both metallic iron as well as Fe_3C (cementite phase iron carbide) (Figure 2). The XRD patterns for the CAs doped with the other iron salts, by contrast, showed reflections consistent with the formation of austenite phase iron carbide ($Fe_{15.1}C$) in addition to metallic iron (Figure 3). In all cases, the diffraction lines became much more pronounced with increasing carbonization temperature, indicating particle coarsening with increasing temperature. We also noted variations in the relative ratios of iron metal to iron carbide for the different Fe-doped CAs. The observed differences in carbide stoichiometry and the relative ratio of iron to iron carbide may arise from the influence that the anion of the Fe salt has on the efficacy of the ion exchange process. The amount of iron incorporated into the aerogel during ion exchange likely determines the amount of metallic iron that evolves during pyrolysis as well as the stoichiometry of iron carbide. This scenario is perhaps substantiated by the observation that the mean crystallite size for the iron particles differs depending on the iron salt used in the preparation of these materials (Table 1). Alternatively, these differences may

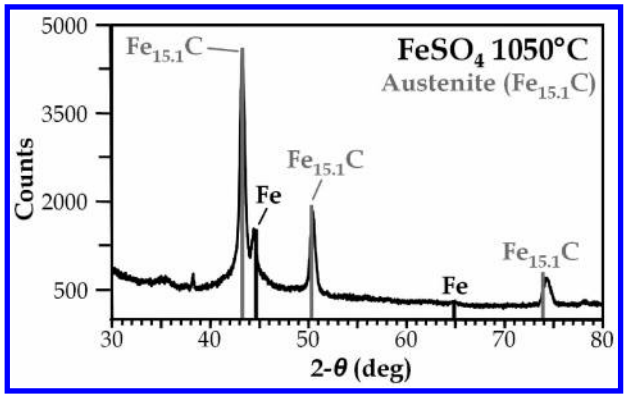

Figure 3. X-ray diffraction patterns for Fe-doped CAs prepared with $FeSO_4$ and the expected peak positions and relative intensities for iron metal and austenite phase of iron carbide.

Table 1. Average Crystallite Sizes of Carbon, Iron, and Iron Carbide Nanoparticles Determined from XRD Spectra and Iron Content Determined by XPS for Undoped and Fe-Doped CAs Carbonized at 1050 °C

precursor salt	mean carbon crystallite size (nm)	mean iron crystallite size (nm)[a]	mean iron carbide crystallite size (nm)[b]	percentage of iron by XPS[c]
$Fe(NO_3)_3$	0.9 ± 0.1	25.8 ± 17.6	21.1 ± 1.7	0.75
$(NH4)_2Fe(SO_4)_2$	1.0 ± 0.1	10.7 ± 1.8	15.0 ± 0.5	0.63
$FeSO_4$	1.0 ± 0.1	20.9 ± 2.0	16.9 ± 0.5	1.33
$FeCl_3$	1.0 ± 0.1	49.4 ± 14.1	58.9 ± 2.3	0.18
undoped	1.0 ± 0.1	ND[d]	ND	0.00

[a] Mean iron crystallite size as determined from the integrated area of the Fe(110) peak. [b] Mean iron carbide crystallite size as determined from the integrated areas of the $Fe_3C(211)$ peak for the cementite-containing sample and from the $Fe_{15.1}C(200)$ peak for the austenite-containing samples. [c] Normalized to percentage by mass of carbon as detected by XPS. [d] ND = not detected.

be related to the residual presence of anions from the iron salts in the aerogels during pyrolysis that can affect particle nucleation and growth during carbonization. The XPS data for the pre-carbonized materials, however, did not show increased concentrations of the elements associated with the anions (i.e., sulfur, nitrogen, or chlorine) relative to the undoped sample. The formation of the Fe species as a function of pyrolysis temperature was examined by XPS (Figure 4). The Fe 2p region of the XPS spectra for CAs pyrolyzed at 600 °C exhibited signals attributable to oxidized iron species, such as FeOOH or Fe_2O_3.[33] Since these oxidized species were not detected in the XRD spectra for these materials, the oxides were likely present as surface coatings on the small clusters of reduced iron species that form during pyrolysis. The Fe 2p XPS spectra for materials pyrolyzed at 800 °C show the emergence of peaks attributable to metallic iron.[33] As the carbonization temperature is increased to 1050 °C, the metallic peaks become more prominent, and the oxide peaks shift to a lower binding energy, suggesting the presence of a reduced oxide such as FeO.[33] On the basis of these trends, the growth of iron and iron carbide nanoparticles likely proceeds through the formation of oxidized intermediates, such as FeOOH and Fe_2O_3. Interestingly, the iron carbide phases were not detected by XPS, indicating that the iron carbide phases probably form inside the carbon aerogel particles.

The XRD spectra for each of the Fe-doped CAs also exhibited a broad diffraction line centered at ~21°, corresponding to the presence of carbon crystallites. The broad nature of the line reflects

(33) Moulder, J. F.; Stickle, W. F.; Sobol, P. E.; Bomben, K. D. *Handbook of X-Ray Photoelectron Spectroscopy*; Physical Electronics Division, Perkin-Elmer Corp.: Eden Prairie, MN, 1992.

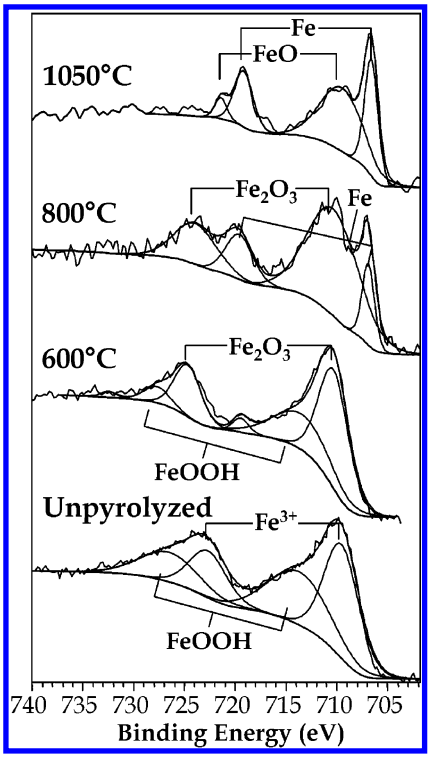

Figure 4. Fe 2p XPS spectra and peak fittings for the unpyrolyzed and pyrolyzed Fe-doped CAs.

the low degree of crystallinity in the aerogel framework for all of the Fe-doped materials. The mean carbon crystallite sizes calculated using the Scherrer equation were found to be between 0.9 and 1.0 nm, independent of pyrolysis temperature or incorporated iron salt (Table 1). Thus, it appears that, despite the presence of iron species, the CA framework does not graphitize appreciably over the range of pyrolysis temperatures investigated. Examination of the carbon structure by Raman spectroscopy supports this observation as well. Raman spectra for carbon aerogels typically show two main features, the ubiquitous G-band (located at ~1580 cm^{-1}) and the disorder-induced D-band (located at ~1360 cm^{-1}).[34] For Fe-doped carbon aerogels, the line widths for these two modes are quite broad, indicating low overall crystallinity of the carbon structure. The approximate carbon crystallite size was calculated from the integrated areas of the D- and G-bands using Knight's formula,[35] $L_\alpha = C_\lambda(I_D/I_G)^{-1}$, where L_α is the average crystallite size, I_D/I_G is the ratio of the integrated area of the D-band to that of the G-band, and C_λ is a fitting parameter that adjusts for the laser wavelength used to generate the spectrum.[36] From this formula, the carbon crystallite sizes were found to be ~2.5 nm for each sample, in reasonably good agreement with the value of ~1.0 nm calculated from the XRD results. As with the XRD data, no change was observed in the carbon crystallite size as a function of pyrolysis temperature, providing further evidence that the carbon structure of the aerogel is not significantly graphitized or otherwise ordered by the presence of Fe during pyrolysis over the temperature range investigated. These results are contrary to our previous work with the Co- and Ni-doped CAs that showed significant graphitization of the carbon structure at temperatures as low as 800 °C. These results also indicate that, unlike the metal particles in Co- and Ni-doped CAs, the Fe-containing nanoparticles present in these materials may be accessible and active for CVD growth of CNTs.

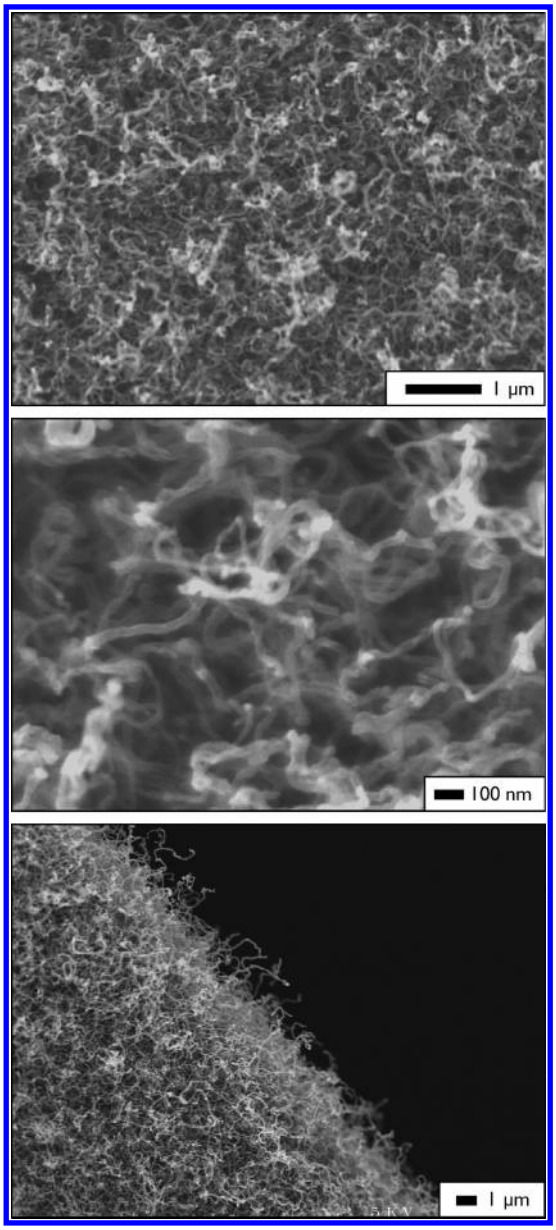

Figure 5. SEM micrographs of Fe800-700 after CVD exhibiting high yield growth of multiwalled CNTs from the CA surface.

Growth of CNTs. The CVD growth of CNTs on the Fe-doped CAs was performed by exposure of the Fe-doped CAs to a flow of CH_4, C_2H_4, and H_2 for a period of 10 min at temperatures ranging from 600 to 800 °C. To determine the Fe-doped CA with the most active Fe catalyst as well as the optimal CVD conditions for CNTs growth on the CAs, each of Fe-doped systems prepared in this study was tested under a variety of CVD conditions. From these experiments, it was determined that the highest yield of CNTs was grown on Fe-doped CAs pyrolyzed at 800 °C and treated at CVD temperatures of 700 °C (Fe800-700). Examination by SEM of the Fe800-700 samples after CVD treatment clearly shows the growth of a grass-like carpet of CNTs on the exterior surface of the CA monolith (Figure 5). The CNTs grown on the Fe800-700 samples appear to be multiwalled with diameters of ~25 nm and lengths up to 4 μm. Analysis of these samples by TEM verifies that the CNTs grown on these CAs are indeed multiwalled (Figure 6). The formation of other tubular graphitic nanostructures, such as nanoribbons and nanoshells, is also

(34) Welsh, I. D.; Sherwood, P. M. A. *Phys. Rev. B* **1989**, *40*, 6386.
(35) Knight, D. S.; White, W. B. *J. Mater. Res.* **1989**, *4*, 385.
(36) Matthews, M. J.; Pimenta, M. A.; Dresselhaus, G.; Dresselhaus, M. S.; Endo, M. *Phys. Rev. B* **1999**, *59*, 6585.

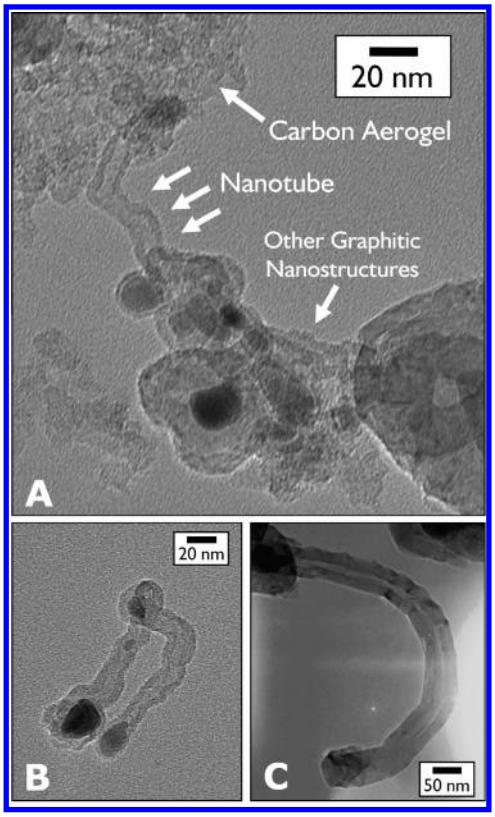

Figure 6. TEM micrographs of Fe800-700 after CVD showing (a) a multiwalled CNT attached to the CA framework and (b and c) CNTs containing embedded catalyst particles detached from the CA monolith.

observed after CVD treatment (bottom portion of Figure 6a). Both SEM and TEM images indicate that the CNTs appear to grow through a tip-growth mechanism, as iron-containing catalyst nanoparticles can be seen at their tips. The observed mean CNT diameter of ~25 nm does not imply that nanoparticles in the CA with smaller or larger diameters do not contribute to nanotube growth. In fact, a range of CNT diameters is observed in the SEM and TEM images for these materials. Nevertheless, the large population of CNTs in this size range suggests that the iron-containing nanoparticles with diameters between 20 and 30 nm possess a suitable chemical composition for catalyzing CNT growth.

Examination of cross-sectioned samples of Fe800-700 by SEM and TEM did not reveal CNT growth beyond a depth of ~1 μm into the porosity of the aerogel. The shallow depth of CVD growth is most likely due to the short mean free path of diffusion intrinsic to mesoporous materials such as aerogels. To address this issue, we attempted to grow CNTs within the interior porosity of the bulk monolith by purging the CA samples with the CVD gases prior to heating. Unfortunately, TEM and SEM analysis of the samples treated by this approach did not show growth of CNTs beyond a depth of about 1 μm from the monolith surface. Nevertheless, we did find that performing CVD on a freshly exposed surface of a Fe-doped CA monolith that had already been processed by CVD resulted in the growth of CNTs on the new surface. Therefore, the limiting factor for CNT growth within the porosity of the CA is indeed the diffusion of CVD gases rather than the activity of the catalyst particles within the CA monolith. To address this issue, we are currently developing new metal-doped CA supports with controlled pore structures that will facilitate diffusion of CVD gases into the interior of the aerogel monoliths and thus enable growth of CNTs throughout the CA structure.

No CNT growth was observed for the Fe600 CA samples. The lack of CNT growth is likely due to the fact that most of the iron in Fe600 is present as an oxide, as evidenced by the XPS spectrum for this material (Figure 4). While exposure of this material to H_2 at elevated temperatures will eventually reduce these iron oxide particles to iron metal, the exposure time used in our CVD process (10 min) was apparently not long enough to produce sufficient amounts of catalytic iron particles. Processing Fe-1050 samples under various CVD conditions resulted in a reduced yield of defective multiwalled CNTs with larger diameters relative to those grown on Fe800 samples. The larger mean diameter of CNTs grown on Fe1050 monoliths is likely due to the presence of larger diameter iron-containing nanoparticles. Growth at CVD temperatures of 800 °C on samples of either Fe800 or Fe1050 resulted in low yields of CNTs (<3 tubes/μm^2) with smaller diameters. Varying the ratio of CVD gases was also found to affect the quality of CNTs grown. For example, decreasing the concentration of methane in the CVD process resulted in the formation of longer, larger diameter CNTs. At the CVD temperatures used for these experiments, methane does not thermolytically crack and instead acts as a carrier gas that dilutes ethylene, the main source of carbon in the CVD reaction. Therefore, the increased size of the CNTs grown under these conditions is most likely due to the relative increase in concentration of ethylene in the feedstock gas.

The CVD results for the various Fe-doped CAs indicate that CNT growth in these materials requires catalyst nanoparticles with a particular size and compositional profile. As a result, metal-doped CAs might serve as an interesting platform for developing a better understanding of CNT growth by heterogeneous catalysis. While iron-based catalysts are commonly used for the growth of CNTs, the exact nature of the catalytic iron species (metallic iron or iron carbide) and its role in CNT growth is still a matter of debate. The approach presented here allows for the growth of supported catalysts of different sizes and compositions and, therefore, can provide insight into the mechanisms of CNT growth.

Conclusion

In this paper, we described the synthesis and characterization of Fe-doped CAs and demonstrate their effectiveness as substrates for the growth of CNTs by CVD. The Fe-doped CAs were found to contain a mixture of iron and iron carbide nanoparticles, the composition and size distributions of which are related to carbonization temperature and the iron salt used to prepare the precursor materials. In addition, the Fe-doped CAs exhibited no observable graphitization of the carbon framework for pyrolysis temperatures up to 1050 °C. CVD processing of the Fe-doped CAs resulted in the surface growth of CNTs, affording novel monolithic carbon aerogel−carbon nanotube composite materials. The thermal and electrical conductivity for these composite materials is currently being investigated. In addition, we are also developing new sol−gel materials with controlled pore structures that will facilitate diffusion of CVD gases into the interior of the aerogel monoliths and thus enable growth of nanotubes throughout the CA structure. This approach could provide a new route to novel materials with enhanced thermal, electrical, and mechanical properties.

Acknowledgment. The authors thank Libby Shaw for her assistance and knowledgeable expertise in performing XPS experiments, Joe Adario for his assistance with XRD, Eduardo Barros for his assistance in collecting HRTEM images, Alfonso Reina for his assistance in collecting SEM images, and Hyungbin Son for his assistance in collecting Raman spectra. The authors

also acknowledge Aerogel Technologies, LLC for use of their supercritical dryers. Work was performed under the auspices of the U.S. Department of Energy by the Lawrence Livermore National Laboratory under Contract W-7405-ENG-48. This research was supported by a LLNL Subcontract B518047 and made use of the Shared Experimental Facilities supported by the MRSEC Program of the National Science Foundation under Award DMR 02-13282.

LA063643M